

DTIC FILE COPY

~~AD-A19032~~

AD

(4)

AD-A190 754

MEMORANDUM REPORT BRL-MR-3639

AERODYNAMIC COEFFICIENT PREDICTIONS  
FOR A PROJECTILE CONFIGURATION AT  
TRANSONIC SPEEDS

C. J. NIETUBICZ  
J. SAHU  
R. LAFARGE

DECEMBER 1987

APPROVED FOR PUBLIC RELEASE; DISTRIBUTION UNLIMITED.

US ARMY BALLISTIC RESEARCH LABORATORY  
ABERDEEN PROVING GROUND, MARYLAND

DTIC  
ELECTE  
FEB 19 1989  
S H D

88 2 19 07 9

UNCLASSIFIED

SECURITY CLASSIFICATION OF THIS PAGE

AD-A190754

## REPORT DOCUMENTATION PAGE

Form Approved  
OMB No 0704-0188  
Exp Date Jun 30 1986

1a REPORT SECURITY CLASSIFICATION UNCLASSIFIED		1b RESTRICTIVE MARKINGS	
2a SECURITY CLASSIFICATION AUTHORITY		3. DISTRIBUTION/AVAILABILITY OF REPORT Approved for public release, distribution unlimited.	
2b DECLASSIFICATION/DOWNGRADING SCHEDULE		5. MONITORING ORGANIZATION REPORT NUMBER(S)	
4. PERFORMING ORGANIZATION REPORT NUMBER(S) BRL-MR-3639		7a. NAME OF MONITORING ORGANIZATION	
6a. NAME OF PERFORMING ORGANIZATION U.S. Army Ballistic Research Laboratory	6b. OFFICE SYMBOL (If applicable) SLCBR-LF	7b. ADDRESS (City, State, and ZIP Code)	
6c. ADDRESS (City, State, and ZIP Code) Aberdeen Proving Ground, Maryland 21005-5066		9. PROCUREMENT INSTRUMENT IDENTIFICATION NUMBER	
8a. NAME OF FUNDING SPONSORING ORGANIZATION	8b. OFFICE SYMBOL (If applicable)	10. SOURCE OF FUNDING NUMBERS	
8c. ADDRESS (City, State, and ZIP Code)		PROGRAM ELEMENT NO 61102A	PROJECT NO 1L161102AH4B
		TASK NO 00	WORK UNIT ACCESSION NO 001 AJ
11. TITLE (Include Security Classification) AERODYNAMIC COEFFICIENT PREDICTIONS FOR A PROJECTILE CONFIGURATION AT TRANSONIC SPEEDS			
12. PERSONAL AUTHOR(S) NIETUBICZ, CHARLES J., SAHU, JUBARAJ, and LAFARGE, ROBERT*			
13a. TYPE OF REPORT Memorandum Report	13b. TIME COVERED FROM _____ TO _____	14. DATE OF REPORT (Year, Month, Day)	15. PAGE COUNT
16. SUPPLEMENTARY NOTATION *Sandia National Laboratory, Albuquerque, New Mexico 27185			
17. COSATI CODES		18. SUBJECT TERMS (Continue on reverse if necessary and identify by block number)	
FIELD 01	GROUP 01	Projectile Aerodynamics, Computational Aerodynamics, Aerodynamic Coefficients, Static Aerodynamic Coefficients, Navier-Stokes Solution, Dynamic Aerodynamic Coefficients	
19. ABSTRACT (Continue on reverse if necessary and identify by block number) This report describes a computational study applied to a M549 projectile configuration. The objective was to apply previously developed Navier-Stokes computational techniques to the M549 shape, compare the results with available experimental data and evaluate the current computational capability. All computations and comparisons are for the transonic flight regime. The projectile flow fields, including the recirculatory base flow regions, were computed using thin-layer Navier-Stokes codes. Increased grid resolution and reduced computational time were achieved by using a vectorized code on a Cray 1S with one million words. Additional results were obtained using the same code on a two million word Cray. Aerodynamic coefficients have been determined from the computed flow fields and are compared to experimental data. The results for the static coefficients show good agreement with the data while the dynamic coefficients such as Magnus moment and roll damping need to be improved.			
20. DISTRIBUTION/AVAILABILITY OF ABSTRACT <input checked="" type="checkbox"/> UNCLASSIFIED-UNLIMITED <input type="checkbox"/> SAME AS RPT <input type="checkbox"/> DTIC USERS		21. ABSTRACT SECURITY CLASSIFICATION UNCLASSIFIED	
22a. NAME OF RESPONSIBLE INDIVIDUAL Charles J. Nietubicz		22b. TELEPHONE (Include Area Code) (301) 278-3591	22c. OFFICE SYMBOL SLCBR-LF-P

# ACKNOWLEDGEMENTS

The vectorized symmetry version of the Navier-Stokes code was made available by Dr. John Benek of Calspan Corporation, Arnold Engineering Development Center, Arnold Air Force Station, Tennessee and is greatly appreciated. The computational funding support for this project by Mr. Don Bohrer of Sandia National Laboratory, Livermore and the computational resource support provided by Mr. Randy Maydew, Sandia National Laboratory, Albuquerque is also appreciated. The computational support provided by Lawrence Livermore Laboratory through the efforts of Ms. Nancy Alexander is appreciated.



Accession For	
NTIS GRA&I	<input checked="" type="checkbox"/>
DTIC TAB	<input type="checkbox"/>
Unannounced	<input type="checkbox"/>
Justification	
By	
Distribution/	
Availability Codes	
Avail and/or	
Dist	Special
A-1	

## TABLE OF CONTENTS

	<u>Page</u>
ACKNOWLEDGEMENTS.....	iii
LIST OF FIGURES.....	vii
I. INTRODUCTION.....	1
II. GOVERNING EQUATIONS AND COMPUTATIONAL TECHNIQUE.....	2
III. MODEL AND COMPUTATIONAL GRIDS.....	3
IV. COMPUTATIONAL CONDITIONS AND CODES.....	4
V. RESULTS.....	5
VI. CONCLUDING REMARKS.....	7
REFERENCES.....	25
LIST OF SYMBOLS.....	26
DISTRIBUTION LIST.....	29

# LIST OF FIGURES

<u>Figure</u>		<u>Page</u>
1	155mm, M549 projectile.....	8
2	Computational model.....	9
3	Grid used with F3D code.....	10
4	Expanded view of grid used with F3D code.....	10
5	Grid used with VSYM3D code - one million words.....	11
6	Grid used with VSYM3D code - two million words.....	11
7	Base region grid.....	12
8a	Mach number contours, $M = .90$ , $\alpha = 2.0$ .....	13
8b	Mach number contours, $M = .95$ , $\alpha = 2.0$ .....	13
9	Aerodynamic coefficient sign convention.....	14
10	Normal force coefficient slope vs Mach number.....	15
11	Pitching moment coefficient slope vs Mach number.....	16
12	Total drag coefficient vs Mach number.....	17
13	Magnus moment slope coefficient vs Mach number.....	18
14	Side force center of pressure vs Mach number.....	19
15	Roll moment coefficient vs Mach number.....	20
16	Summation of pitching moment coefficient vs body length.....	21
17	Leeward surface pressure vs longitudinal position, F3D, VSYM3D(1M), VSYM3D(2M), $M = .95$ , $\alpha = 2.0$ .....	22

## I. INTRODUCTION

The flight of projectiles covers a wide range of speeds. The capability to predict the aerodynamic behavior in transonic and supersonic flow is essential to the design of new projectiles or in the modification of existing shapes. In recent years a considerable research effort has been focused on the development of modern predictive capabilities for determining projectile aerodynamics. The general approach taken has been to apply the thin-layer Navier-Stokes solvers in both a space marching and time marching manner to the supersonic and transonic flow fields respectively.

At supersonic speeds Sturek and Schiff<sup>1</sup> have successfully applied a Parabolized Navier-Stokes code to predict the flow field about an ogive-cylinder-boattail body. The resultant aerodynamic coefficients were found to be in very good agreement with the available experimental data. This work has been further advanced to include the effects of a blunt nose configuration<sup>2</sup> which more closely resembles an actual fielded artillery round. The initial emphasis has been on developing a specific capability for predicting projectile aerodynamics. This computational capability is most useful in the eventual design and evaluation process. Towards this end a computational parametric study has been performed by Sturek and Mylin<sup>3</sup> and trends in the aerodynamic coefficients were determined.

The transonic regime represents an area in which a similar computational capability is being sought. The critical aerodynamic behavior which occurs between Mach  $\approx .90$  and 1.2 is always of concern in the development of shell. For the transonic regime the time dependent thin-layer Navier-Stokes technique has been applied to projectile configurations for axisymmetric flow conditions.<sup>4</sup> A base flow version of the code has also been developed.<sup>5</sup> Agreement with experimental data for the surface pressures has been very good. The base flow calculations show correct qualitative features of the flow field. The extension of these techniques to a fully three dimensional flow field which exists on a spinning projectile at angle of attack has recently been reported.<sup>6</sup> The normal force coefficient was shown to be in good quantitative agreement with the available experimental data. The Magnus force predictions were not as encouraging but did show the correct development of Magnus force along the body.

This computational study utilizes the developed time dependent thin-layer Navier-Stokes computational technique to compute the static and dynamic aerodynamic coefficients for a standard M549 artillery shell. The initial objective was to obtain a series of computational results which cover the critical Mach number range and determine the applicability of these codes as a predictive tool. Three versions of the thin-layer Navier-Stokes codes were used: (a) a full three dimensional version (F3D); (b) vectorized symmetry version (VSYM3D), and (c) a axisymmetric base flow version. The full range of aerodynamic coefficients, which includes base drag have been determined. The computed results are compared to a set of experimental data which combines both wind tunnel and range data. All computations for which the aerodynamic coefficients are presented were obtained on the Sandia National Laboratory Cray 1S which has one million words of memory. Results from computations obtained on the 2M word Cray 1S at Lawrence Livermore National Laboratory, are also shown.

## II. GOVERNING EQUATIONS AND COMPUTATIONAL TECHNIQUE

The governing equations solved are the unsteady thin-layer Navier-Stokes equations. The thin-layer approximation, which neglects the viscous gradients in the longitudinal and circumferential direction, has been applied to a variety of problems with very good results. The transformed equations written in strong conservation law form for the full 3D (Eq. (1)) and axisymmetric formulation (Eq. (2)) are

$$\frac{\partial \hat{q}}{\partial \tau} + \frac{\partial \hat{E}}{\partial \xi} + \frac{\partial \hat{F}}{\partial \eta} + \frac{\partial \hat{G}}{\partial \zeta} = \frac{1}{Re} \frac{\partial \hat{S}}{\partial \zeta} \quad (1)$$

$$\frac{\partial \hat{q}}{\partial \tau} + \frac{\partial \hat{F}}{\partial \xi} + \frac{\partial \hat{G}}{\partial \zeta} + \hat{H} = \frac{1}{Re} \frac{\partial \hat{S}}{\partial \zeta} \quad (2)$$

respectively. The general coordinate transformations are defined as

$\xi = \xi(x, y, z, t)$  = is the longitudinal coordinate

$\eta = \eta(x, y, z, t)$  = is the circumferential coordinate

$\zeta = \zeta(x, y, z, t)$  = is the near normal coordinate

$\tau$  = time

The vector  $\hat{q}$  contains the dependent variables ( $\rho, \rho u, \rho v, \rho w, e$ ) and the flux vectors  $\hat{E}, \hat{F}, \hat{G}$  contain terms which arise from the conservation of mass, momentum and energy in the three coordinate directions. The source vector  $\hat{H}$  contain terms which result from an analytic determination of the flux vector  $\hat{F}$  given the assumptions of axisymmetric flow and a constant angular velocity. The viscous terms are contained in the vector  $\hat{S}$  which is seen to have variation in the  $\zeta$  direction only. This represents the thin-layer approximation mentioned earlier.

The numerical scheme used for the solution of Equations (1) and (2) is a fully implicit, approximately factored, finite difference algorithm in delta form as analysed by Beam and Warming.<sup>7</sup> The solution is implemented by an approximate factorization which allows the system of equations to be solved in three successive one dimensional steps for the 3D problem and two one dimensional steps for the axisymmetric formulation. Details of the numerical method, computational algorithm and boundary conditions can be found in References 6 and 8.

### III. MODEL AND COMPUTATIONAL GRIDS

The actual projectile configuration for which these simulations were run is shown in Figure 1. There are certain features on this projectile, such as the flat nose and rotating band, which can not yet be modeled exactly. Therefore a modified configuration as shown in Figure 2, was used for the computations. The flat nose was modeled as a hemisphere cap and the rotating band was omitted. Recent results have been presented by Danberg<sup>9</sup> for supersonic flow wherein the rotating band was modeled as a ramp function and the results compared well the experimental data. This work is presently being extended to for the transonic regime.

Equations (1) and (2) are solved in a transformed coordinate space thus allowing for a wide variation in body geometry. The body configuration is introduced through the determination of the metric terms  $\xi_x$ ,  $\eta_x$ ,  $\zeta_x$ , etc. and the Jacobian. These terms are formed by a combination of the derivative terms  $x_\xi$ ,  $y_\xi$ ,  $z_\xi$ . One of the first steps in performing a computation is the generation of a stationary computational grid for the metric determination. These points are determined prior to the computations and are not changed with time. Three grids were used in this study for the 3D calculations and one grid for the base flow results. All 3D grids were generated using a projectile grid generation code<sup>10</sup> which solves either elliptic or by hyperbolic differential equations.

The grid used for the full 3D run is shown in Figures 3 and 4 consisted of 60 longitudinal, 24 normal and 36 circumferential points. The overall grid was extended to 18 calibers in front, above and behind the projectile body. This is required to insure that imposed free stream boundary conditions are satisfied and that waves are not reflected back into the computational domain. This type of computational space has also been verified by a series of axisymmetric calculations. An expanded view of the grid is shown in Figure 4 and shows the details of longitudinal and radial grid point clustering required for the shock and viscous resolution respectively. The wake has been modeled as an extended sting for the 3D calculations. The base flow code models the base regime and calculates the wake and resulting base pressure.

A second grid, shown in Figure 5, was developed for the symmetry calculations and contained 80 longitudinal, 32 normal and 21 grid points in the circumferential half plane. Only the static aerodynamic coefficients can be determined with this grid since bi-lateral symmetry conditions are imposed. Thus the full three dimensional flow field which exists for a spinning projectile at angle of attack cannot be determined. Grid points for both cases were clustered on the boattail to resolve the expected asymmetric shock pattern. The shock asymmetry and possible base region influence are felt to be the major contributions to the critical aerodynamic behavior. Only the static aerodynamic coefficients can be determined, however since this grid imposes a bi-lateral symmetry condition. Thus the full three dimensional flow field which exists for a spinning projectile at angle of attack cannot be determined. These two grids made use of the full one million word memory capacity on the Sandia Cray 1S.

A third grid was generated, for a symmetry calculation run on the Lawrence Livermore Cray 1S with two million words, and is shown in Figure 6.

This machine enabled a grid of 110 longitudinal, 32 normal and 21 circumferential points to be generated. The fine resolution in the longitudinal direction is evident from this figure and improved results are expected. The aerodynamic coefficients for this last case have not yet been computed however, a preliminary result of the pressure distribution along the surface will be shown.

A final grid, generated using a hybrid grid generation code, was used for the base flow calculations and is shown in Figure 7. Grid points are shown to be clustered in the base region and although it has not been used here the capability exists to have the base grid adapt to the shear layer as it develops.<sup>11</sup>

#### IV. COMPUTATIONAL CONDITIONS AND CODES

An objective of this effort was to computationally determine the magnitude and trends of the static and dynamic aerodynamic coefficients where the critical behavior is known to exist, namely between Mach = .90 through 1.2. The following table is a summary of the conditions and codes used for the computations.

MACH NO.	(Re $\times 10^{-6}$ )	F3D	VSYM3D	BASE FLOW
.90	2.2	X	X	X
.95	2.32	X	X	X
.98	2.39	X	X	X
1.05	2.56		X	X
1.10	2.69		X	X
1.20	2.93		X	X

A large number of runs were made during this study using the full 3D and vectorized symmetry 3D Navier-Stokes code on the Sandia National Laboratory Cray 1S. The computations for base pressure were all performed at the Ballistic Research Laboratory, Aberdeen Proving Ground, Maryland on the CDC 7600. The run times for the 3D cases were quite large. The F3D code ran at .00055 sec/time step/point and required 1000 steps for convergence. Thus each case ran about 6.9 hours on the Cray. The VSYM3D ran at .00011 sec/time step/point and required 2500 time step for convergence. The total run time per case for this version was 3.1 hours.

The two codes differed in the operational aspect with the F3D being more robust than the VSYM3D. Lower values of smoothing parameters (explicit smoothing/ $\Delta t \approx 1.6$ ) and higher values of  $\Delta t$  ( $\approx .05$ ) were able to be used for the F3D code while a smoothing value of  $\approx 4.0$  and maximum  $\Delta t \approx .03$  were required for the VSYM3D code. The lower  $\Delta t$  thus caused the VSYM3D to require

more time steps for convergence. Additionally the convergence histories for the F3D runs were favorable in that the residual decrease and time increases did not cause the solution to diverge repeatedly. A very careful approach to changing times and smoothing was required for the VSYM3D runs to avoid the solution becoming unstable. However, for the cases with Mach > 1 the F3D code became very unstable and solutions were not obtained. The cause of the instability was due to the shock system forming in front of the nose. Additional local smoothing would have been required to obtain a solution.

## V. RESULTS

The VSYM3D code was used to determine the static coefficients only, since bi-lateral symmetry was imposed and the projectile could not spin. The F3D code was used to determine the flow fields for the spinning cases from which the static and dynamic coefficients could be obtained. Qualitative features, resulting from the F3D calculations, are shown in Figures 8a and 8b, where the Mach contours have been plotted for  $M = .90$  and  $M = .95$  respectively. The supersonic regions are clearly seen in these figures as well as the asymmetry of the shock positions due to the projectile being at angle of attack. The longitudinal asymmetry and shock interaction with the base region flow field are believed to cause the critical behavior in the aerodynamic coefficients over the transonic range.

The resultant flow field calculations were integrated to determine the aerodynamic coefficients. The results to be presented here include the static coefficients: normal force slope, pitching moment slope, and center of pressure. The dynamic coefficients presented include: Magnus moment slope, side force center of pressure, and roll moment slope. The sign convention used is shown in Figure 9. The normal force is shown to act in the plane of the angle of attack while the Magnus force acts in the plane normal to the angle of attack. The Magnus moment is shown to act about the normal force axis while the pitching moment acts about the side force axis. The slope of the moment coefficients ( $C_{M_{p\alpha}}$ ,  $C_{M_{\alpha}}$ ) are presented, however, since it is those terms which

are used to determine stability criteria. The computed results are compared with experimental data<sup>12</sup> which are a compilation of wind tunnel and range data for the XM549 shape.

The static aerodynamic coefficients for normal force slope, pitching moment slope and center of pressure are shown as a function of Mach number in Figures 10, 11, and 12 respectively. The results from both codes, the F3D and VSYM3D are compared with the experimental data. The primary difference in the two codes to be considered here is the total number and distribution of grid points. The VSYM3D version allows more points to be used in the longitudinal and normal directions than that for the F3D version. The circumferential point distribution has been fixed at  $\Delta\phi = 10^\circ$  for both versions. The normal force slope has been shown to depend on the number of circumferential points by Klopfer and Chaussee.<sup>13</sup> This work showed that the normal force slope continued to change until points were used every  $10^\circ$  in the circumferential plane. That same criteria was used for this work.

The normal force slope coefficient is shown in Figure 10 for both the computational results and experimental data. The experimental data is shown

to decrease as it approaches a critical Mach number ( $M = .95$ ) and then shows a rapid increase throughout the remaining transonic regime. The F3D computational results agree well above  $M = .95$  however, it over predicts the data below  $M = .95$ . The VSYM3D results show an improved agreement with the experimental data except at  $M = 1.2$ . The increased number of grid points was expected to provide better agreement and generally has predicted the correct trend for  $C_{N_\alpha}$ .

The pitching moment slope coefficient is generally of greater concern in projectile aerodynamics. Figure 11 shows the pitching moment slope comparison for the computations and the experimental data. Here the F3D results are found to be in general agreement with the magnitude of the experimental data but show very little effect of Mach number. The inability to predict the Mach number effect is attributed to the insufficient number of grid points along the body. The VSYM3D computations however show a very definite trend with Mach number. This is a result of being able to capture more accurately the expansion regions and shock structure with the increased resolution. Although the magnitude of the VSYM3D results do not agree with the experimental data, the prediction of the trend with Mach number is very encouraging and was one of the objectives of this study.

The total drag of a projectile configuration results from summation of the pressure, viscous, and base drag components. The 3D codes were used to obtain the pressure and viscous contributions to drag since the base was modeled as an extended sting. The base drag was obtained by running the base flow (axisymmetric) code at  $\alpha = 0.0^\circ$ . The total drag was then determined by adding all the components described above. The only effect not accounted for in this approach is the change in base drag due to angle of attack. Figure 12 compares the total drag coefficients for both computations against the experimental data. The F3D results do show a reasonable agreement with the data however they are inconclusive due to the limited number of calculations performed in this critical Mach number region. The VSYM3D results cover a wider range and tends to predict the drag rise associated with transonic flow. The magnitude at  $M = 1.05$  and  $M = 1.2$  does not agree with the experimental data. Although the pressure drag component had increased at  $M = 1.2$ , the base drag was still predicting a significant contribution. The difference between the experimental data and calculations are most likely due to the overprediction of the base drag.

The dynamic coefficients of Magnus moment slope, side force center of pressure and roll moment are shown in Figures 13, 14, and 15 respectively. The flow field computations for these coefficients required the F3D code since a projectile at angle of attack with spin is a fully three dimensional problem with no plane of symmetry. The critical aerodynamic behavior is shown experimentally to exist for the dynamic coefficients as well. The experimental results presented in Figure 13 show the Magnus moment slope to change significantly throughout the transonic regime. The computed results however show almost no change in the Magnus moment coefficient with Mach number. This large change in aerodynamic coefficients is in part attributed to the longitudinal asymmetry of the shock position. This has not been captured by the present computation due to the poor grid resolution in the boattail region. The Magnus force center of pressure is shown in Figure 14 and although shows some change with respect to the Mach number variation is considered to be only

a marginal result. The Magnus effect is a result of the viscous interaction and resulting skewed displacement surface which exists about a spinning projectile at angle of attack. Therefore adequate resolution of the viscous boundary layer is essential for good results. An indication of the inadequate viscous resolution for these computations is shown in Figure 15 where the roll moment coefficient has been plotted as function of Mach number. The roll moment is strictly a result of the viscous effects and thus is a much more sensitive indicator of the viscous resolution than the Magnus force. The poor agreement shown here is therefore directly attributed to the insufficient grid resolution in the boundary layer. Using the full capacity of the CRAY 1S allowed for only 24 points between the body and the outer boundary of 18 calibers.

The longitudinal distribution of points is also very critical to the determination of shock position and eventually to the determination of the pressure acting on the body surface. Figure 16 is a plot of the accumulative pitching moment as a function of position on the model for various Mach numbers. The pitching moment on the nose is seen to be the same for all Mach numbers. The largest effect is shown to occur at the ogive cylinder junction and on the boattail. With the boattail having such a dramatic effect on the aerodynamic coefficients, good resolution of the boattail flow field is essential. A few runs were made on the Lawrence Livermore Laboratory, CRAY 1S with two million words, using the grid shown in Figure 6. A plot of the pressure distribution acting on the leeward surface is presented in Figure 17 for the F3D, VSYM3D (one million) and VSM3D (two million) runs. With the increased resolution a sharper definition of the shock, indicated by a more rapid rise in pressure, is seen on the cylinder ( $X/D \approx 3.8$ ) and on the boattail ( $X/D \approx 5.5$ ). This pressure distribution is expected to provide a more accurate prediction of the aerodynamic coefficients.

## VI. CONCLUDING REMARKS

Three versions of the unsteady thin-layer Navier-Stokes codes were applied to the standard M549 projectile configuration. The full 3D version, F3D, was used to determine the static and dynamic aerodynamic coefficients as a function of Mach number. The vectorized symmetry 3D version, VSYM3D, was used to determine the static coefficients. A base flow version was used to compute the base drag. The computed coefficients have been compared to a set of experimental data. The static coefficients predicted the correct trends with the experimental data while the dynamic coefficients did not. The critical aerodynamic behavior was found to be qualitatively predicted when sufficient longitudinal grid points were made available by using the symmetry version of the code. Additional work is required in resolving the viscous effects of a spinning projectile at angle of attack.



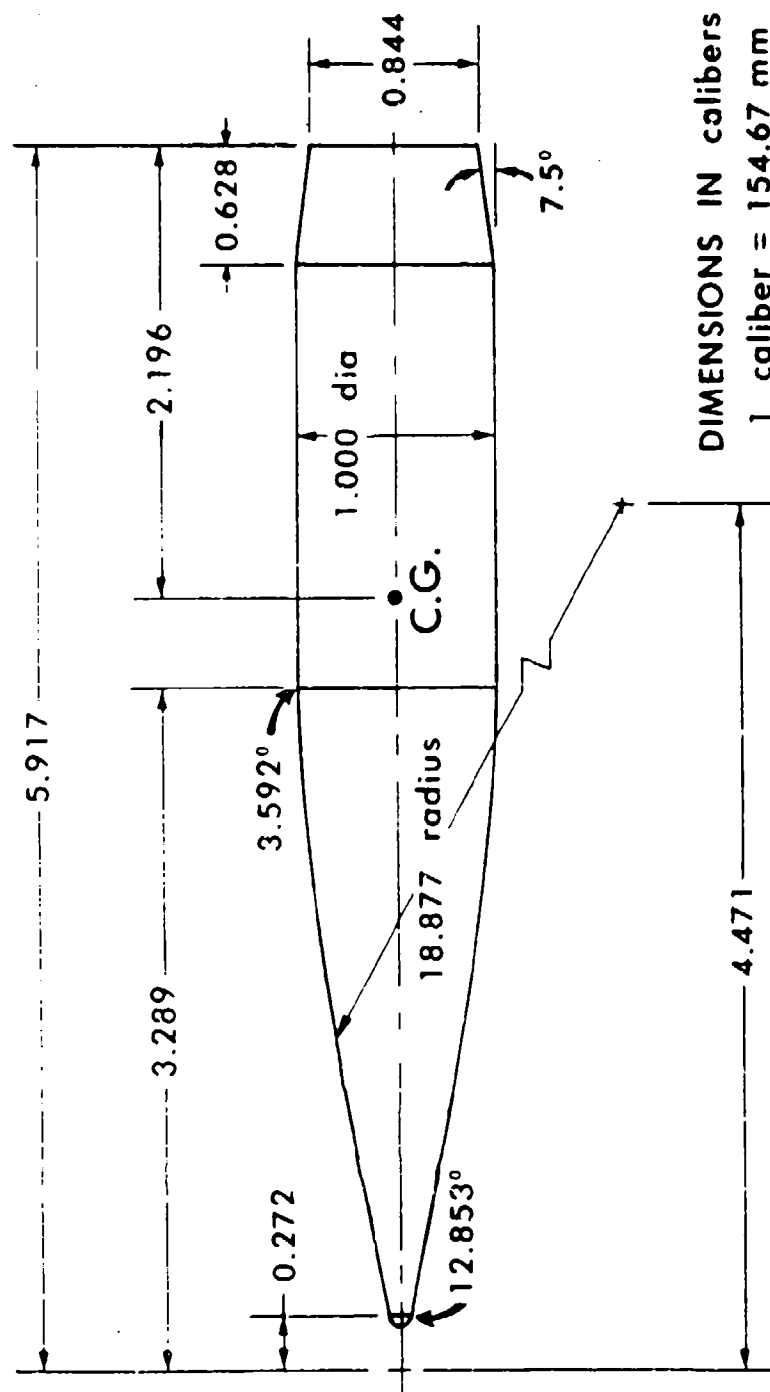


Figure 2. Computational model.

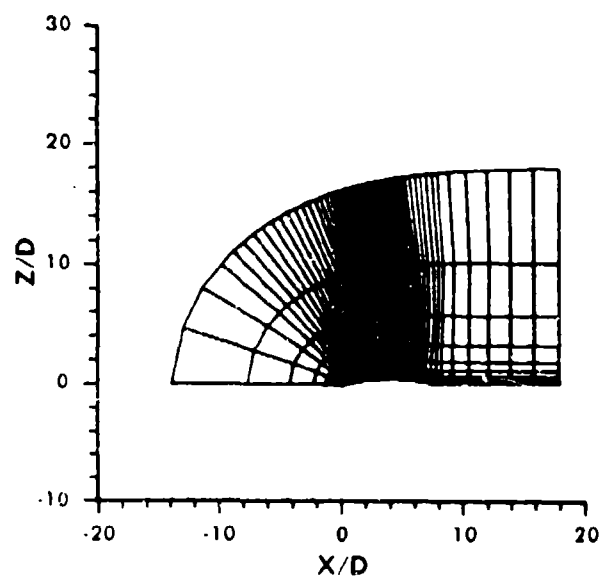


Figure 3. Grid used with F3D code.

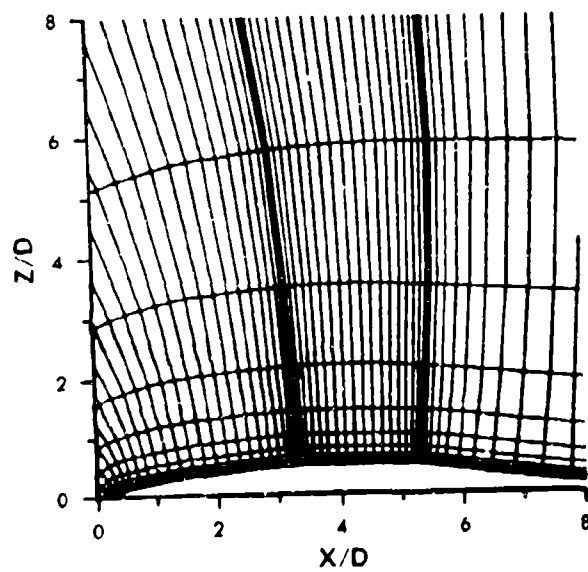


Figure 4. Expanded view of grid used with F3D code.

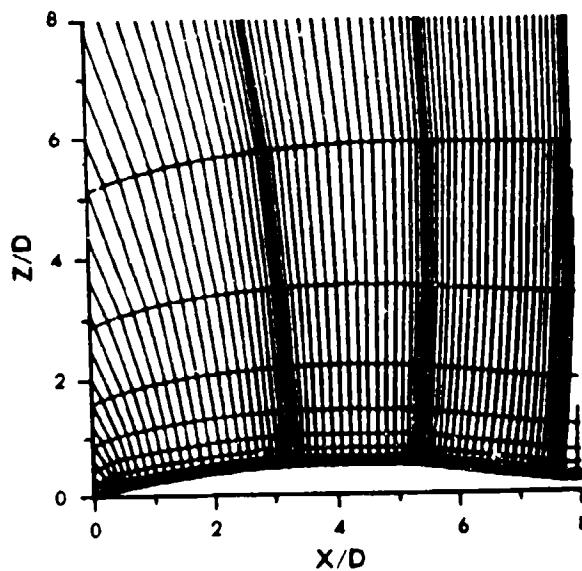


Figure 5. Grid used with VSYM3D code - one million words.

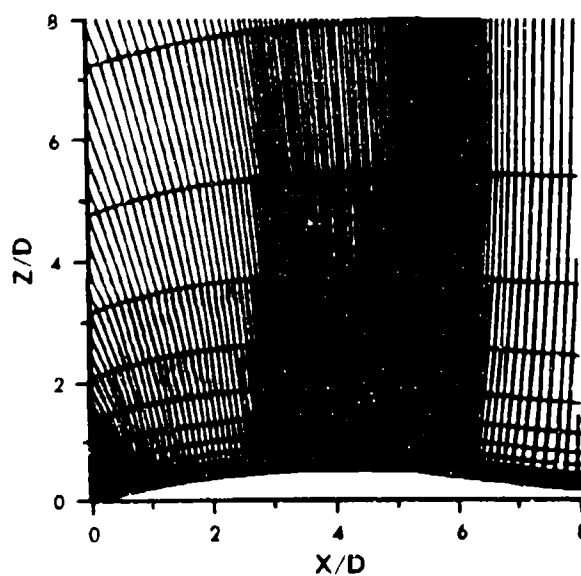


Figure 6. Grid used with VSYM3D code - two million words.

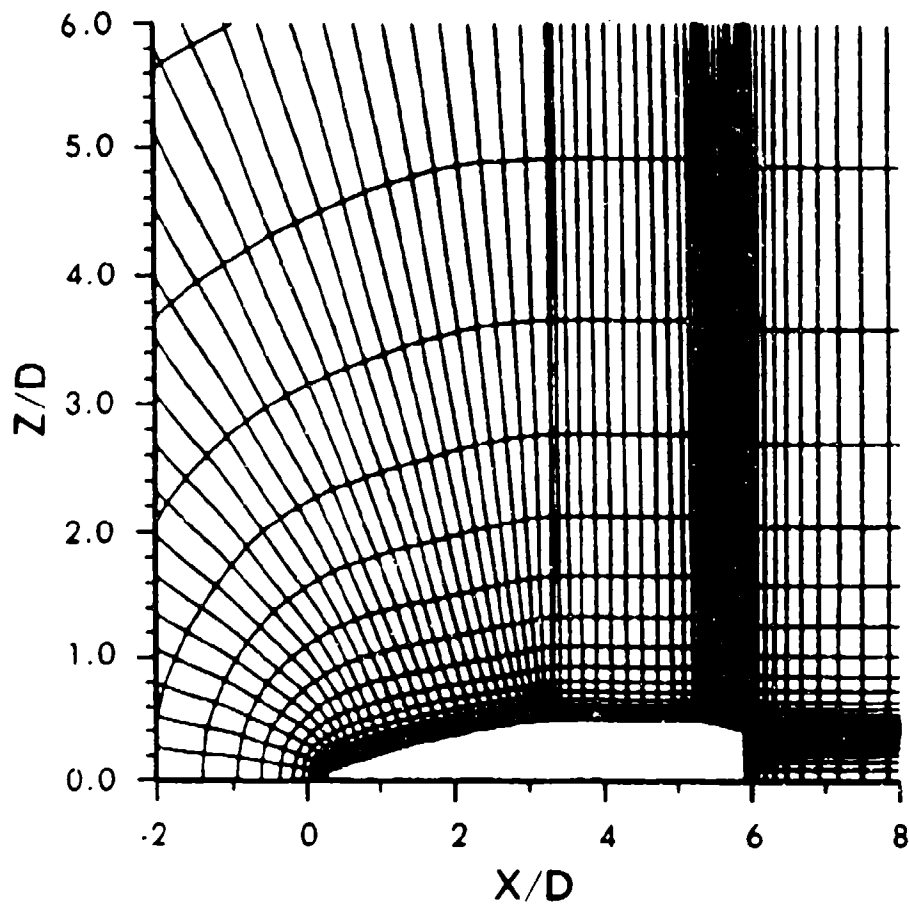


Figure 7. Base region grid.

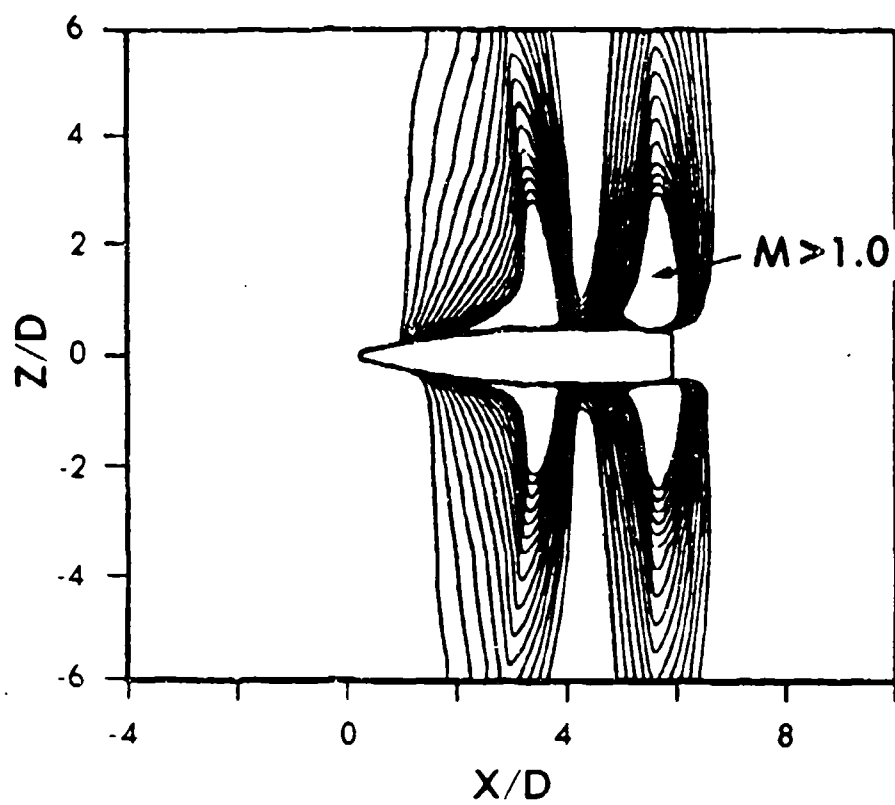


Figure 8a. Mach number contours,  $M = .90$ ,  $\alpha = 2.0$ .

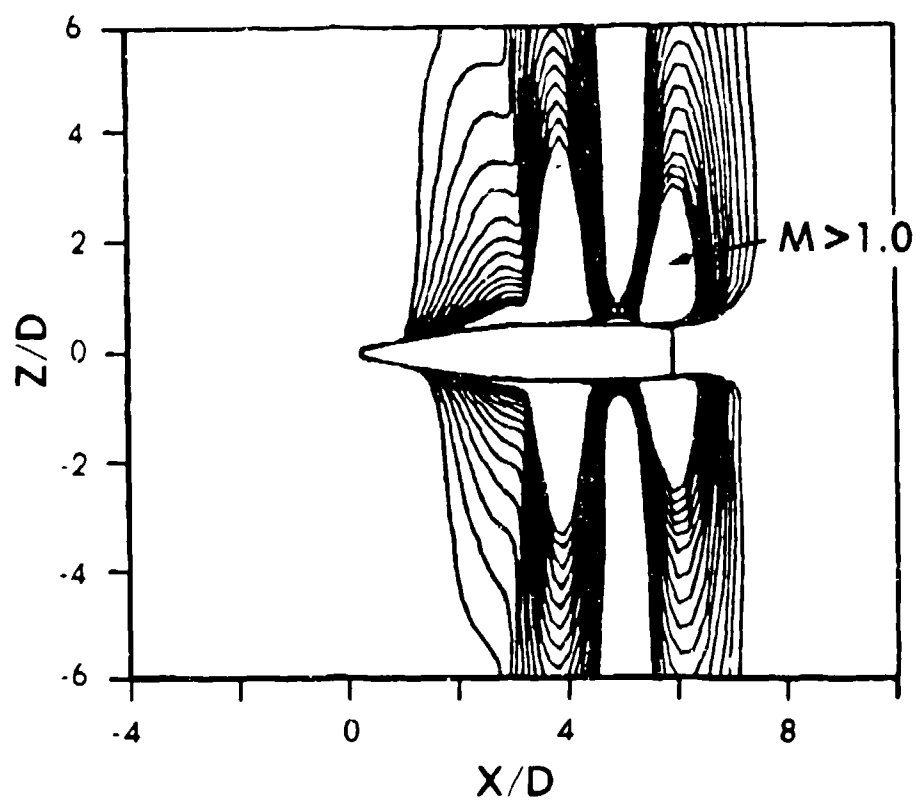


Figure 8b. Mach number contours,  $M = .95$ ,  $\alpha = 2.0$ .

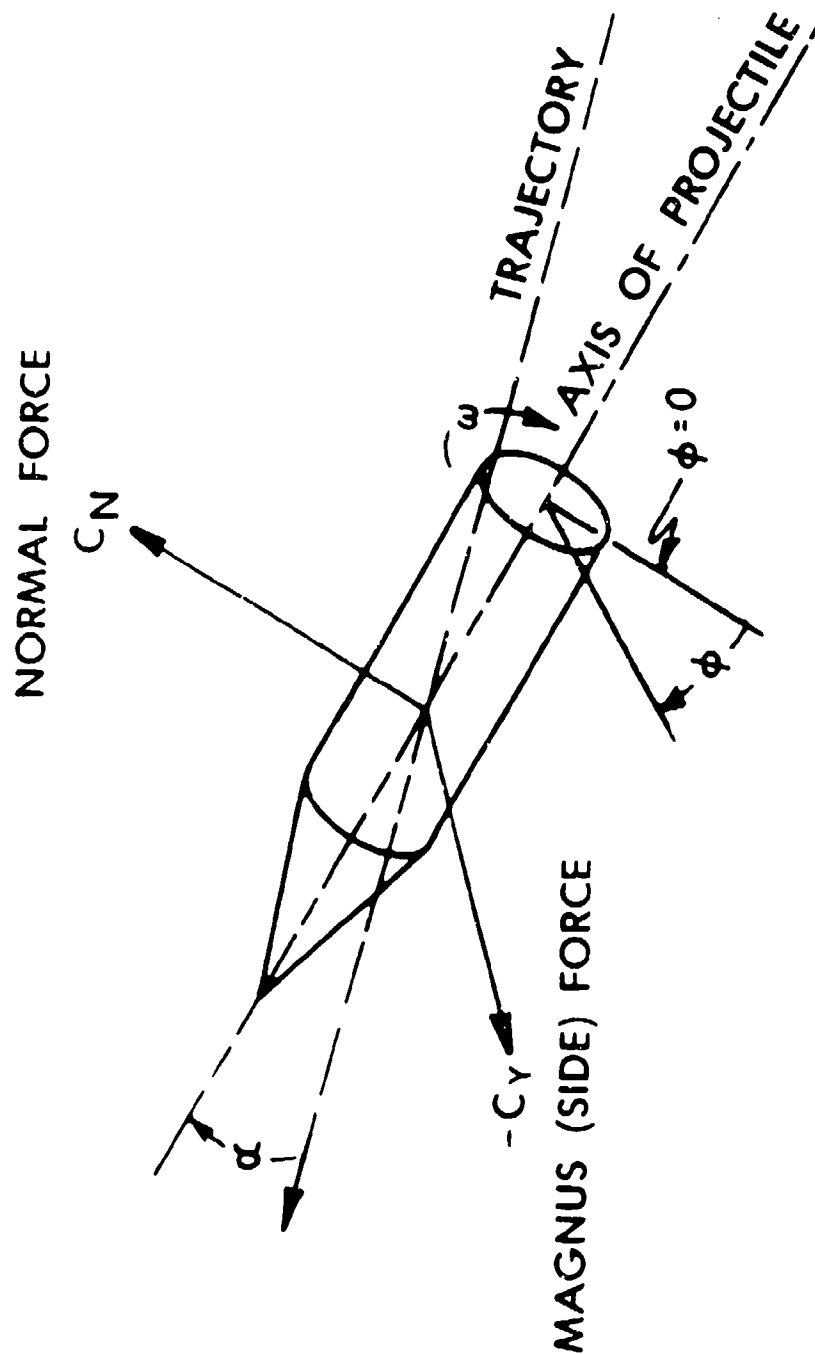


Figure 9. Aerodynamic coefficient sign convention.

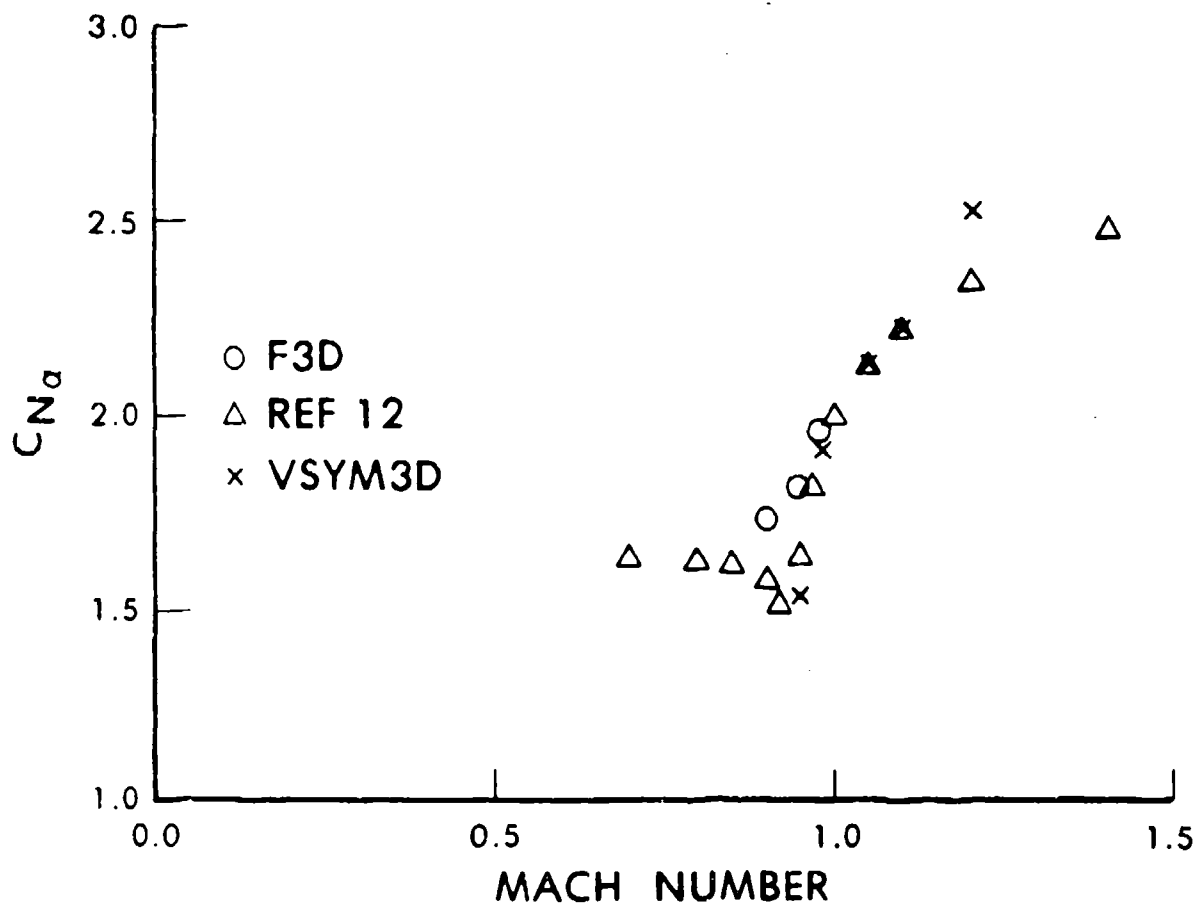


Figure 10. Normal force coefficient slope vs Mach number.

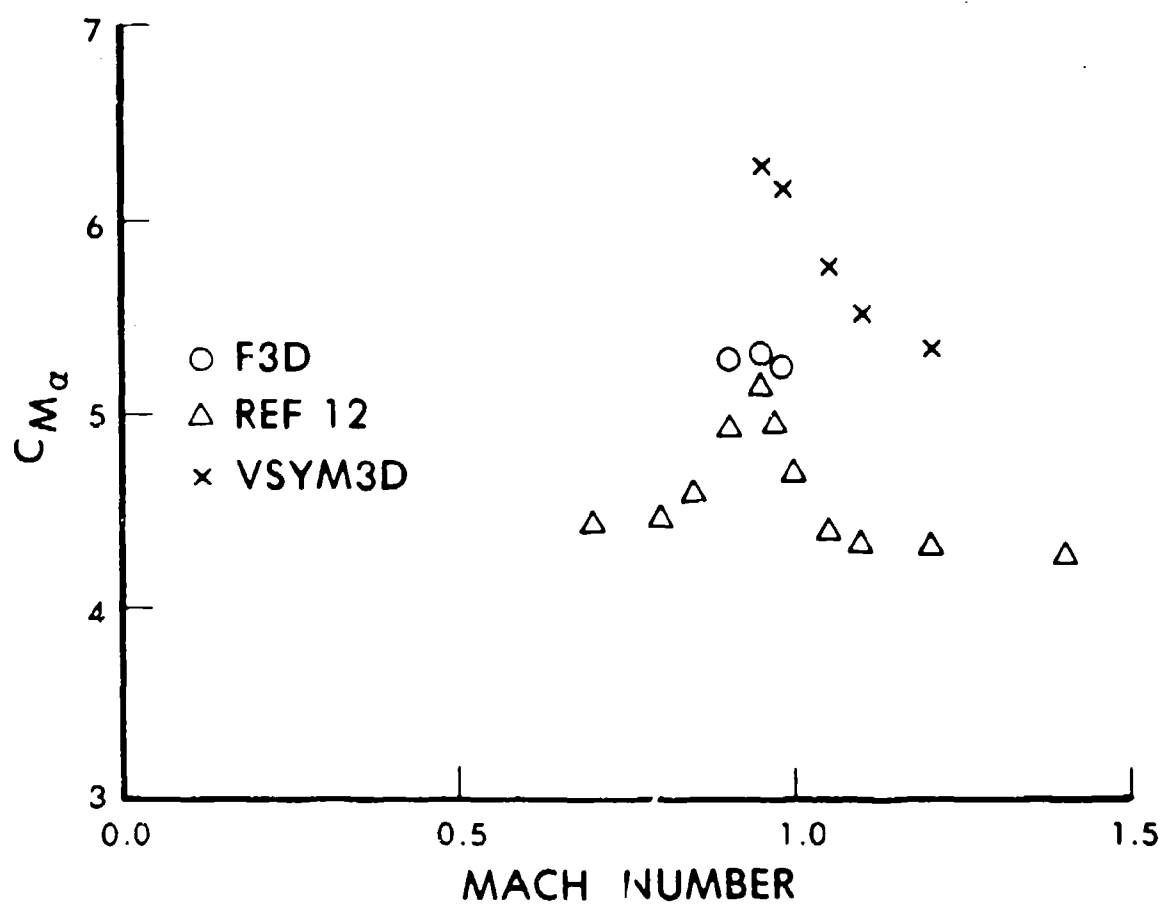


Figure 11. Pitching moment coefficient slope vs Mach number.

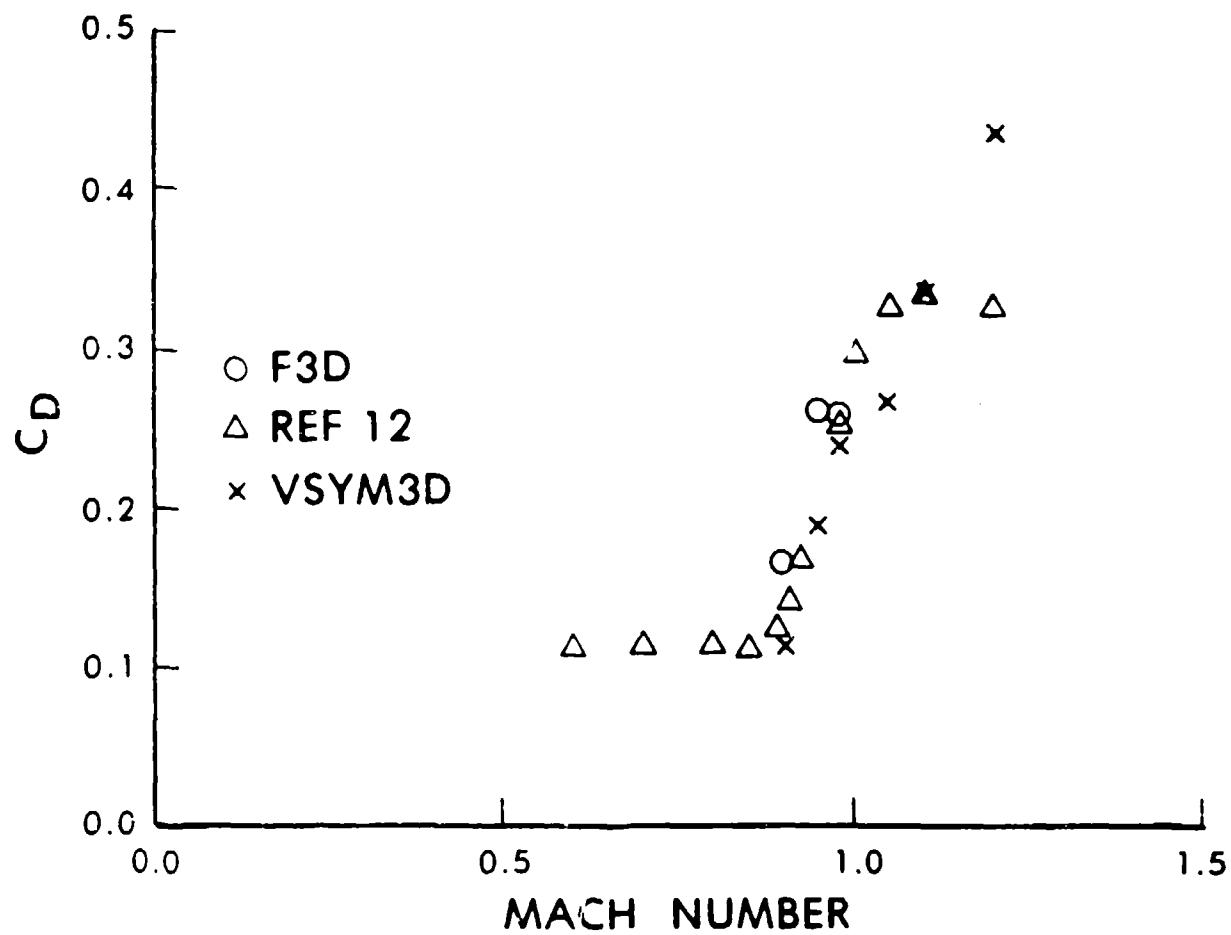


Figure 12. Total drag coefficient vs Mach number.

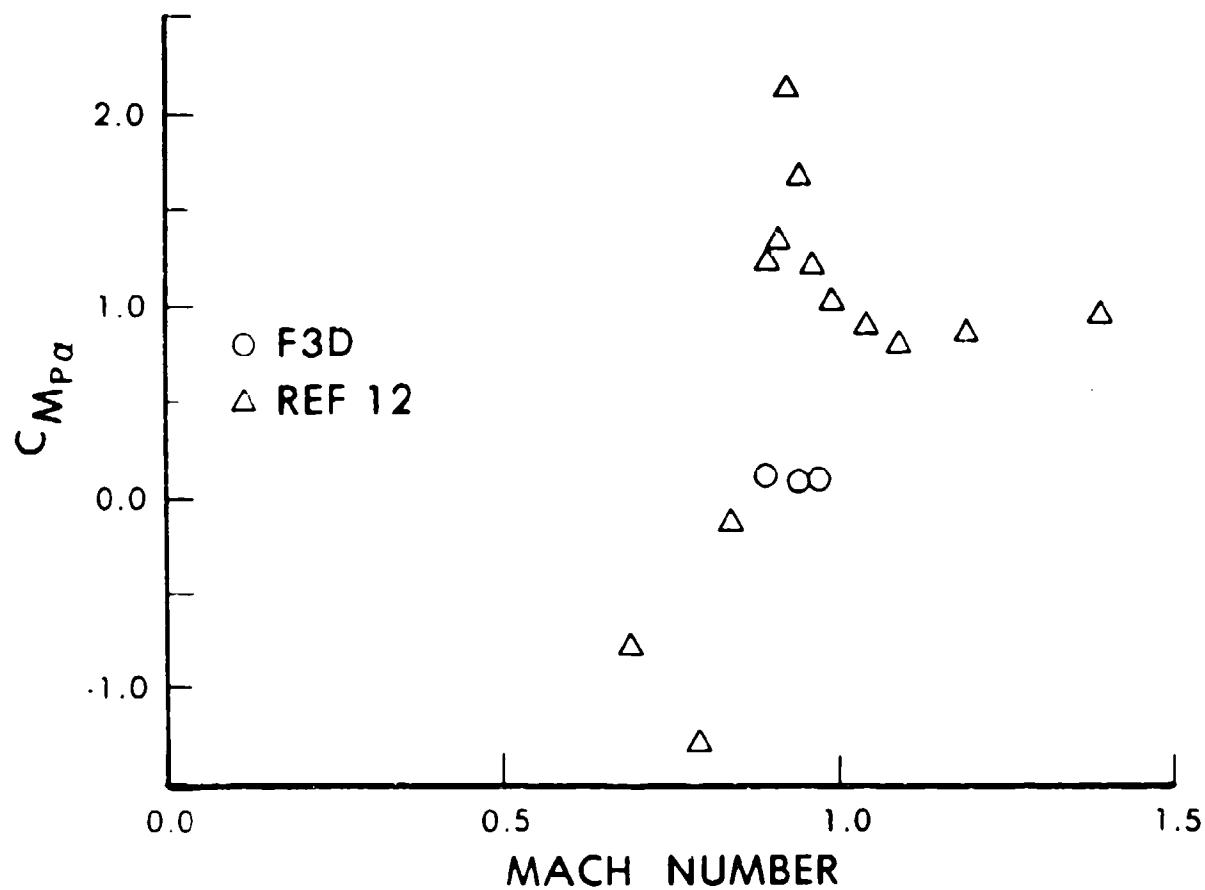


Figure 13. Magnus moment slope coefficient vs Mach number.

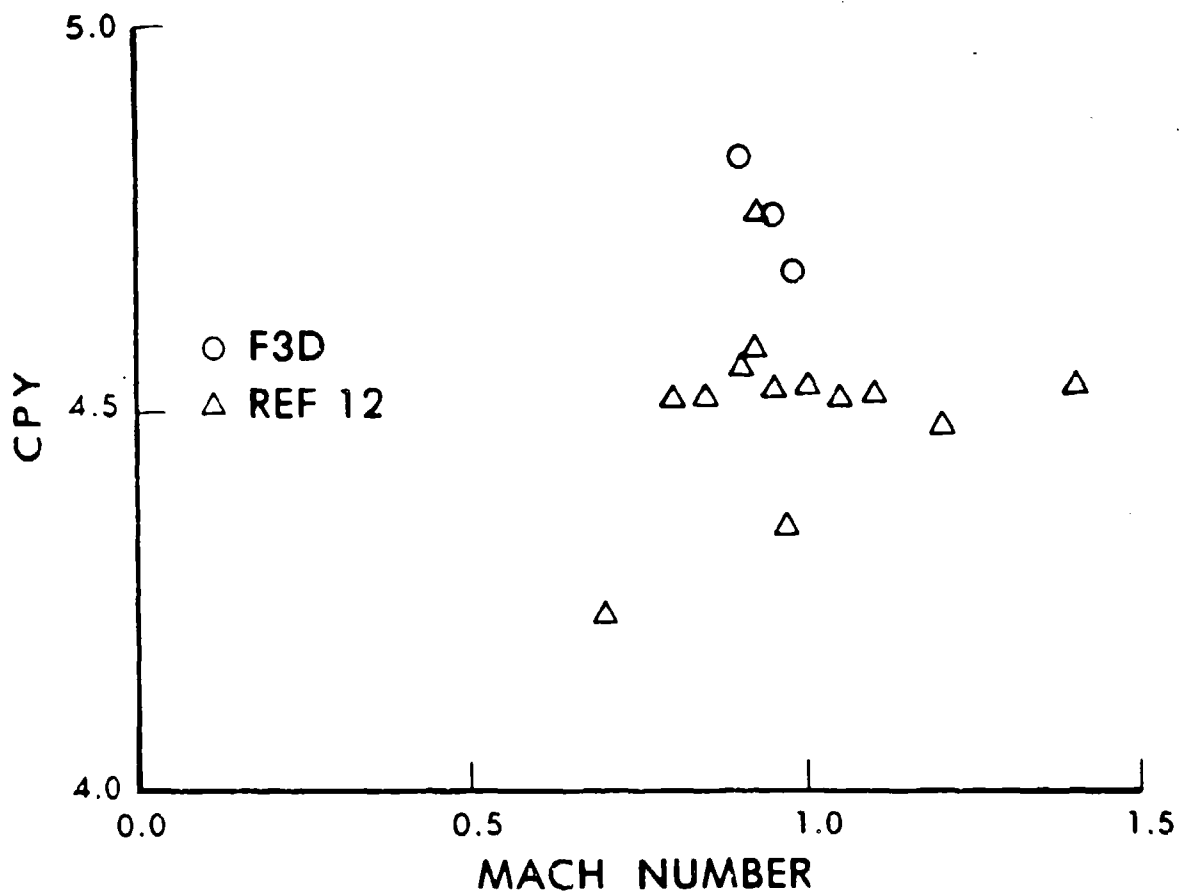


Figure 14. Side force center of pressure vs Mach number.

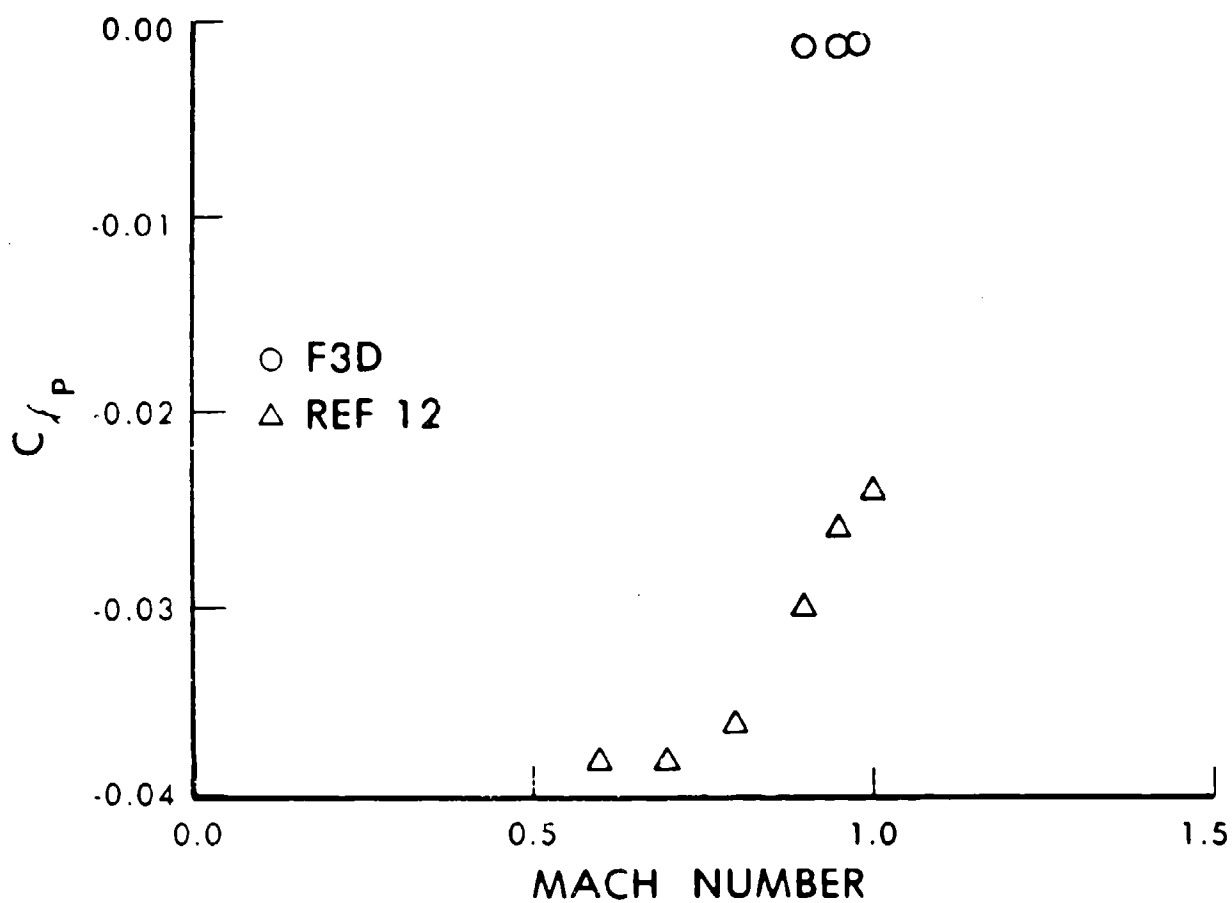


Figure 15. Roll moment coefficient vs Mach number.

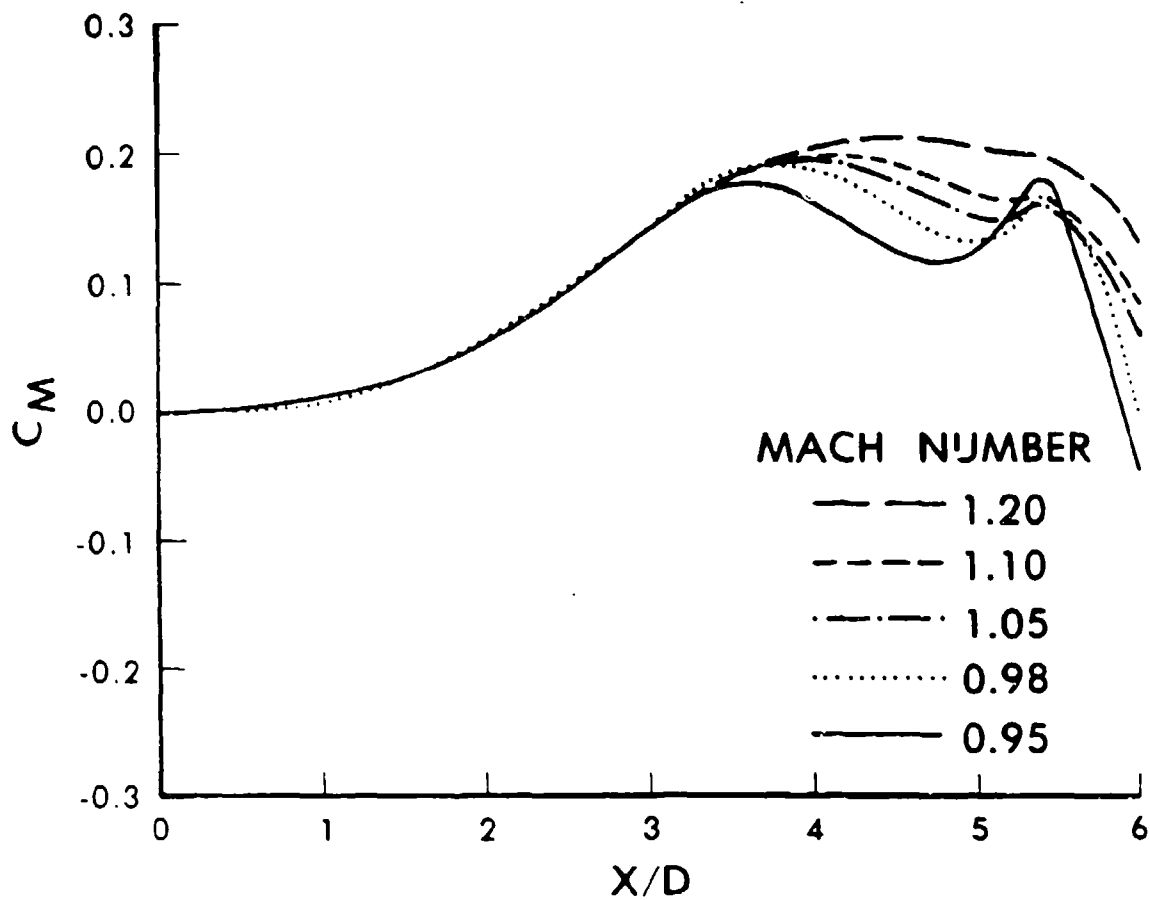


Figure 16. Summation of pitching moment coefficient vs body length.

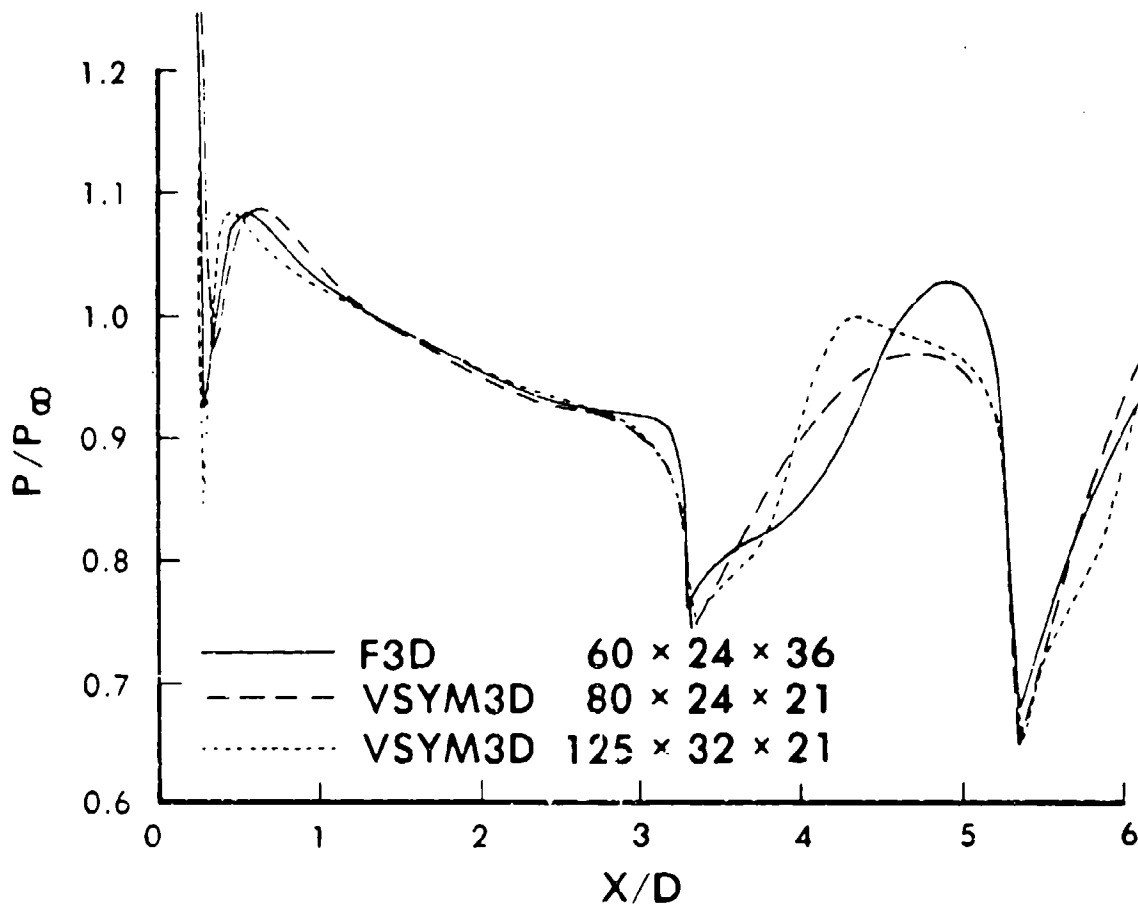


Figure 17. Leeward surface pressure vs longitudinal position, F3D, VSYM3D(1M), VSYM3D(2M),  $M = .95$ ,  $\alpha = 2.0$ .

## REFERENCES

1. Schiff, L.B. and Steger, J.L., "Numerical Simulation of Steady Supersonic Viscous Flow," AIAA Journal, Vol. 18, No. 12, December 1980, pp. 1421-1430.
2. Sturek, W.B., Guidos, B., and Nietubicz, C.J., "Navier-Stokes Computational Study of the Magnus Effect on Shell with Small Bluntness at Supersonic Speeds," AIAA Paper No. 82-1341, AIAA Flight Mechanics Conference, August 1982.
3. Sturek, W.B. and Mylin, D.C., "Computational Parametric Study of the Magnus Effect on Boattailed Shell at Supersonic Speeds," AIAA Paper No. 81-1900, AIAA Atmospheric Flight Mechanics Conference, August 1981.
4. Nietubicz, C.J., "Navier-Stokes Computations for Conventional and Hollow Projectile Shapes at Transonic Velocities," AIAA Paper No. 81-1262, AIAA 14th Fluid and Plasma Dynamics Conference, Palo Alto, CA, 1981.
5. Sahu, J., Nietubicz, C.J., and Steger, J.L., "Numerical Computation of Base Flow for a Projectile at Transonic Speeds," AIAA Paper No. 82-1358, AIAA Flight Mechanics Conference, August 1982.
6. Nietubicz, C.J., Sturek, W.B., and Heavey, K.R., "Computations of Projectile Magnus Effect at Transonic Velocities," AIAA Paper No. 83-0237, Aerospace Sciences Meeting, January 1983.
7. Beam, R. and Warming, R.F., "An Implicit Factored Scheme for the Compressible Navier-Stokes Equations," AIAA Paper No. 77-645, June 1977.
8. Nietubicz, C.J., Pulliam, T.H., and Steger, J.L., "Numerical Solution of the Azimuthal-Invariant Thin-Layer Navier-Stokes Equations," ARBRL-TR-02227, U.S. Army Ballistic Research Laboratory, Aberdeen Proving Ground, Maryland, March 1980. (AD A085716)
9. Danberg, J.E., "Numerical Modeling of Rotating Band Flow Field and Comparison with Experiment," ARBRL-TR-02505, U.S. Army Ballistic Research Laboratory, Aberdeen Proving Ground, Maryland, July 1983. (AD A131260)
10. Nietubicz, C.J., Heavey, K.R., and Steger, J.L., "Grid Generation Techniques for Projectile Configurations," Proceedings of 1982 Army Numerical Analysis and Computers Conference, ARO Report 82-3, February 1982.
11. Sahu, J., Nietubicz, C.J., and Steger, J.L., "Navier-Stokes Computations of Projectile Base Flow with and without Base Injection," AIAA Paper No. 83-0224, Aerospace Sciences Meeting, January 1983.
12. Kline, R., Herrmann, W.R., and Oskay, V., "A Determination of the Aerodynamic Coefficients of the 155mm, M549 Projectile," TR-4764, Picatinny Arsenal, Dover, New Jersey, November 1974. (AD B002073)
13. Klopfer, G.H. and Chaussee, D.S., "Numerical Solution of Three-Dimensional Transonic Flows Approved Axisymmetric Bodies at Angle of Attack," 11th U. S. Navy Symposium on Aeroballistics, Philadelphia, PA, 22-24 August 1978.

# LIST OF SYMBOLS

$a$	= speed of sound
$CP$	= center of pressure for normal force
$CPY$	= center of pressure for Magnus force
$C_{\ell_p}$	= roll damping
$C_m$	= pitching moment coefficient
$C_{M_{p\alpha}}$	= $d^2C_n/[d(\frac{PD}{V}) \cdot d\alpha]$ , slope of Magnus moment coefficient evaluated at $PD/V = 0, \alpha = 0$
$C_{M_\alpha}$	= $dC_m/d\alpha$ , slope of pitching moment coefficient evaluated at $\alpha = 0$
$C_n$	= Magnus (yawing) moment coefficient
$C_N$	= normal force coefficient
$C_{N_\alpha}$	= $dC_N/d\alpha$ , slope of normal force coefficient evaluated at $\alpha = 0$
$C_Y$	= Magnus (side) force
$d$	= local diameter of model
$D$	= reference diameter of model
$\hat{E}, \hat{F}, \hat{G}$	= flux vectors of transformed gasdynamic equation
$\hat{H}$	= source term vector
$L$	= reference length
$M$	= Mach number
$p$	= pressure normalized by $\rho_\infty a_\infty^2$
$\hat{q}$	= vector of dependent variables
$\omega D/V$	= non-dimensional spin rate about model axis
$Re$	= Reynolds number $\rho_\infty a_\infty D/\mu_\infty$
$\hat{S}$	= viscous flux vector
$u, v, w$	= Cartesian velocity components along the x, y, z axis, respectively, normalized by $a_\infty$

## LIST OF SYMBOLS (Continued)

$\alpha$  = angle of attack

$\xi, \eta, \zeta$  = computational coordinates in the axial, circumferential, and radial directions

$\rho$  = density, normalized by free-stream density  $\rho_\infty$

### Subscripts

$\infty$  = free-stream conditions

$\Omega$  = spin rate about model axis, rad/sec

# DISTRIBUTION LIST

<u>No. of Copies</u>	<u>Organization</u>	<u>No. of Copies</u>	<u>Organization</u>
12	Administrator Defense Technical Info Center ATTN: DTIC-FDAC Cameron Station, Bldg 5 Alexandria, VA 22304-6145	1	Director US Army Aviation Research and Technology Activity Ames Research Center Moffett Field, CA 94035-1099
1	HQDA DAMA-ART-M Washington, DC 20310	10	C.I.A. OIR/DB/Standard GE47 HQ Washington, DC 20505
1	Commander US Army Materiel Command ATTN: AMCDRA-ST 5001 Eisenhower Avenue Alexandria, VA 22333-0001	1	Commander US Army Communications - Electronics Command ATTN: AMSEL-ED Fort Monmouth, NJ 07703-5301
2	Commander US Army Armament Research, Development and Engineering Center ATTN: SMCAR-MSI SMCAR-LCA-F/Hudgins Dover, NJ 07801-5001	1	Commander CECEOM R&D Technical Library ATTN: AMSEL-IM-L (Reports Section) B.2700 Fort Monmouth, NJ 07703-5000
1	Commander US Army Armament, Research, Development and Engineering Center ATTN: SMCAR-TDC Dover, NJ 07801-5001	1	Commander US Army Missile Command Research, Development, and Engineering Center ATTN: AMSMI-RD Redstone Arsenal, AL 35898-5230
1	Commander US AMCCOM ARDEC CCAC Benet Weapons Laboratory ATTN: SMCAR-CCB-TL Watervliet, NY 12189-4050	1	Director US Army Missile and Space Intelligence Center ATTN: AIAMS-YDL Redstone Arsenal, AL 35898-5500
1	Commander US Army Armament, Munitions and Chemical Command ATTN: AMSMC-IMP-L Rock Island, IL 61299-7300	1	Commander US Army Tank Automotive Command ATTN: AMSTA-TSL Warren, MI 48397-5000
1	Commander US Army Aviation Systems Command ATTN: AMSAV-ES 4300 Goodfellow Blvd St. Louis, MO 63120-1798	1	Director US Army TRAIDOC Analysis Center ATTN: ATOR-TSL White Sands Missile Range, NM 88002-5502

# DISTRIBUTION LIST

<u>No. of Copies</u>	<u>Organization</u>	<u>No. of Copies</u>	<u>Organization</u>
2	Commander US Naval Surface Weapons Center ATTN: Dr. T. Clare, Code DK20 Dr. F. Moore Dahlgren, VA 22448-5000	1	University of California, Davis Department of Mechanical Engineering ATTN: Prof. H.A. Dwyer Davis, CA 95616
1	Commandant US Army Infantry School ATTN: ATSH-CD-CS-OR Fort Benning, GA 31905-5400	1	Virginia Polytechnic Institute & State University ATTN: Dr. Clark H. Lewis Department of Aerospace & Ocean Engineering Blacksburg, VA 24061
1	Commander US Army Development and Employment Agency ATTN: MODE-ORO Fort Lewis, WA 98433-5000	1	Commandant USAFAS ATTN: ATSF-TSM-CN Fort Sill, OK 73503-5600
1	AFWL/SUL Kirtland AFB, NM 87117		<u>Aberdeen Proving Ground</u>
1	Air Force Armament Laboratory ATTN: AFATL/DLODL (Tech Info Center) Eglin AFB, FL 32542-5000		Dir, USAMSAA ATTN: AMXSU-D AMXSU-MP, H. Cohen
4	Director NASA Ames Research Center ATTN: MS-202A-14/Kutler MS-202-1/Pulliam Steger MS-227-8/Schiff Moffett Field, CA 94035		Cdr, USATECOM ATTN: AMSTE-SI-F
2	Sandia Laboratories ATTN: Dr. W.L. Oberkamp Dr. F. Blottner Division 1636 Sandia National Laboratories Albuquerque, NM 87185		Cdr, CRDC, AMCCOM ATTN: SMCCR-RSP-A SMCCR-MU SMCCR-SPS-IL
1	AEDC Calspan Field Services ATTN: MS 600 (Dr. John Benek) AAFS, TN 37389		
1	Bendix Guided Systems Division ATTN: MS 2/17A/Wasserman Teterboro, NJ 07608		

# USER EVALUATION SHEET/CHANGE OF ADDRESS

This Laboratory undertakes a continuing effort to improve the quality of the reports it publishes. Your comments/answers to the items/questions below will aid us in our efforts.

1. BRL Report Number \_\_\_\_\_ Date of Report \_\_\_\_\_

2. Date Report Received \_\_\_\_\_

3. Does this report satisfy a need? (Comment on purpose, related project, or other area of interest for which the report will be used.) \_\_\_\_\_  
\_\_\_\_\_  
\_\_\_\_\_

4. How specifically, is the report being used? (Information source, design data, procedure, source of ideas, etc.) \_\_\_\_\_  
\_\_\_\_\_  
\_\_\_\_\_

5. Has the information in this report led to any quantitative savings as far as man-hours or dollars saved, operating costs avoided or efficiencies achieved, etc? If so, please elaborate. \_\_\_\_\_  
\_\_\_\_\_  
\_\_\_\_\_

6. General Comments. What do you think should be changed to improve future reports? (Indicate changes to organization, technical content, format, etc.) \_\_\_\_\_  
\_\_\_\_\_  
\_\_\_\_\_

CURRENT  
ADDRESS

\_\_\_\_\_  
Name  
\_\_\_\_\_  
Organization  
\_\_\_\_\_  
Address  
\_\_\_\_\_  
City, State, Zip

7. If indicating a Change of Address or Address Correction, please provide the New or Correct Address in Block 6 above and the Old or Incorrect address below.

OLD  
ADDRESS

\_\_\_\_\_  
Name  
\_\_\_\_\_  
Organization  
\_\_\_\_\_  
Address  
\_\_\_\_\_  
City, State, Zip

(Remove this sheet, fold as indicated, staple or tape closed, and mail.)